

Likelihood Assignment for Out-of-Distribution Inputs in Deep Generative Models is Sensitive to Prior Distribution Choice

Ryo Kamoi, Kei Kobayashi
Keio University, Japan

ryo_kamoi_st@keio.jp, kei@math.keio.ac.jp

Abstract

Recent work has shown that deep generative models assign higher likelihood to out-of-distribution inputs than to training data. We show that a factor underlying this phenomenon is a mismatch between the nature of the prior distribution and that of the data distribution, a problem found in widely used deep generative models such as VAEs and Glow. While a typical choice for a prior distribution is a standard Gaussian distribution, properties of distributions of real data sets may not be consistent with a unimodal prior distribution. This paper focuses on the relationship between the choice of a prior distribution and the likelihoods assigned to out-of-distribution inputs. We propose the use of a mixture distribution as a prior to make likelihoods assigned by deep generative models sensitive to out-of-distribution inputs. Furthermore, we explain the theoretical advantages of adopting a mixture distribution as the prior, and we present experimental results to support our claims. Finally, we demonstrate that a mixture prior lowers the out-of-distribution likelihood with respect to two pairs of real image data sets: Fashion-MNIST vs. MNIST and CIFAR10 vs. SVHN.

1. Introduction

The out-of-distribution detection is an important area of study that has attracted considerable attention [28, 11, 21, 31] to improve the safety and reliability of machine learning systems. Detection methods based on density estimation using a parametric model have been studied for low dimensional data [28], and deep generative models seem to be a reasonable choice when dealing with high-dimensional data. However, recent work [23, 12, 31, 24, 5] has shown that deep generative models such as VAEs [18], PixelCNN [34], and flow-based models [8, 16] cannot distinguish training data from out-of-distribution inputs in terms of the likelihood. For instance, deep generative models trained on Fashion-MNIST assign higher likelihoods to MNIST than

to Fashion-MNIST, and those trained on CIFAR-10 assign higher likelihood to SVHN than to CIFAR-10 [23]. Methods for mitigating this problem have been proposed from various perspectives [12, 2, 5, 24].

We focus on the influence of the prior distribution of deep generative models on the likelihood assigned to out-of-distribution data. Although the typical choice is a standard normal distribution, various studies have analyzed alternatives [7, 4, 33, 35]. However, present work mainly focuses on the representative ability and the likelihood assigned to in-distribution data when evaluating prior distributions. To the best of our knowledge, no existing work has analyzed the effect that the prior distribution has on the likelihood assigned to out-of-distribution inputs. Here, we consider data sets that can be naturally partitioned into clusters, so the underlying distribution can be approximated by a multimodal distribution with modes apart from each other. This assumption is reasonable for many data sets found in the wild such as Fashion-MNIST, which contains different types of images, including T-shirts, shoes, and bags. If a unimodal prior distribution is used to train generative models on such data sets, the models are forced to learn the mapping between unimodal and multimodal distributions. We consider this inconsistency an important factor underlying the assignment of high likelihood to out-of-distribution areas.

We use untrainable mixture prior distributions and manually allocate similar data to each component before training by using labels of data sets or k-means clustering. Under these conditions, the models trained on Fashion-MNIST successfully assign lower likelihoods to MNIST. Our approach also lowers the likelihoods assigned to SVHN by models trained on CIFAR-10. We provide three explanations for our observations. First, as mentioned above, a multimodal prior distribution can alleviate the inconsistency between a prior and a data distribution, which is a possible factor underlying the out-of-distribution problem. Second, allocating similar data to each component can reduce the possibility of accidentally assigning undesirable out-of-distribution points to high likelihood areas. Our second or-

der analysis can theoretically justify this intuition in a manner similar to the work of Nalisnick *et al.* [23]. Third, out-of-distribution points are forced out of high likelihood areas of the prior distribution when a multimodal prior is used. Somewhat surprisingly, the out-of-distribution phenomenon still occurs when a model with a unimodal prior is trained only on data that would be allocated to one component in the multimodal case. This is a novel observation that motivates further investigation of designing the latent variable space to mitigate the out-of-distribution phenomenon.

2. Related Work

Our work is directly motivated by the recent observation that deep generative models can assign higher likelihoods to out-of-distribution inputs [23, 5]. The use of prior distributions has been studied independently of this line of work.

2.1. Out-of-Distribution Detection by Deep Generative Models

Although model likelihood is often used to evaluate deep generative models, Theis *et al.* [32] showed that high likelihood is neither sufficient nor necessary for models to generate high quality images. Remarkably, Nalisnick *et al.* [23] has reported that deep generative models such as VAEs, flow-based models, and PixelCNN can assign higher likelihoods to out-of-distribution inputs. Similar phenomena have also been reported in parallel studies [5, 12].

Solutions have been proposed from various perspectives. Hendrycks *et al.* [12] proposed “outlier exposure”, a technique that uses carefully chosen outlier data sets during training to lower the likelihood assigned to out-of-distribution inputs. Bütepage *et al.* [2] focused on VAEs and reported that the methods for evaluating likelihood and the assumption of a visual distribution on pixels influence the likelihood assigned to out-of-distribution inputs. Another line of study is to use alternative metrics. Choi *et al.* [5] proposed using the Watanabe-Akaike Information Criterion (WAIC) as an alternative. Nalisnick *et al.* [24] hypothesized that out-of-distribution points are not located in the model’s “typical set”, and thus proposed the use of a hypothesis test to check whether an input resides in the model’s typical set.

2.2. Prior distribution

A typical choice for a prior distribution for deep generative models such as VAEs and flow-based models is a standard Gaussian distribution. However, various studies have proposed the use of different alternatives. One line of study selects more expressive prior distributions, such as multimodal distributions [15, 7, 33, 25, 14], stochastic processes [25, 10, 3], and autoregressive models [4, 35]. Another option is to use discrete latent variables [29, 35]. Previous work on the choice of the prior distribution for deep

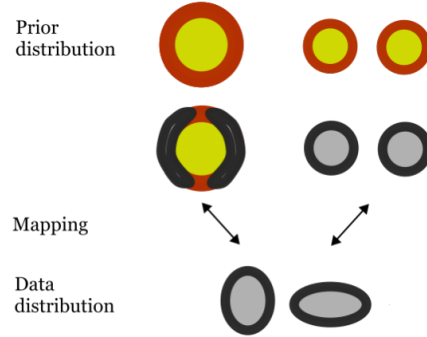


Figure 1: Motivation for using a multimodal prior distribution from a topological point of view. If the prior distribution is mapped to a distribution with a different topology, the mapped distribution will inevitably have undesirable high likelihood areas. The black and red areas represent the typical sets of the prior and the data distribution, respectively. The gray and yellow areas represent high likelihood areas of the prior and the data distribution, respectively. While the distributions are shown in two-dimensions in this figure, this inconsistency between high likelihood areas and typical sets is a problem observed in high dimensional data.

generative models have focused on the representative ability, natural fit to data sets, and the likelihood or reconstruction of in-distribution inputs. To the best of our knowledge, no previous study has focused on the relationships between the prior distribution and the likelihood assigned to out-of-distribution data.

3. Motivation

In this section, we discuss the theoretical motivations for using a multimodal prior distribution; topology mismatch and second order analysis. On a related note, we have observed that a multimodal prior distribution can force out-of-distribution points out of high likelihood areas. We explain this effect in Section 5.3.

3.1. Topology Mismatch

We focus on data sets that have “clusters”, and adopt an assumption that the underlying distribution can be approximated as a multimodal distribution with components located far away from each other. We analyze deep generative models by approximating them as topology-preserving invertible mappings between a prior distribution and a data distribution. Nalisnick *et al.* [24] focused on the “typical set” [6] of deep generative models and the data distribution. As suggested by Nalisnick *et al.* [24], here, we assume that deep generative models learn mappings from the typical set of the prior distribution to the typical set of the data distribu-

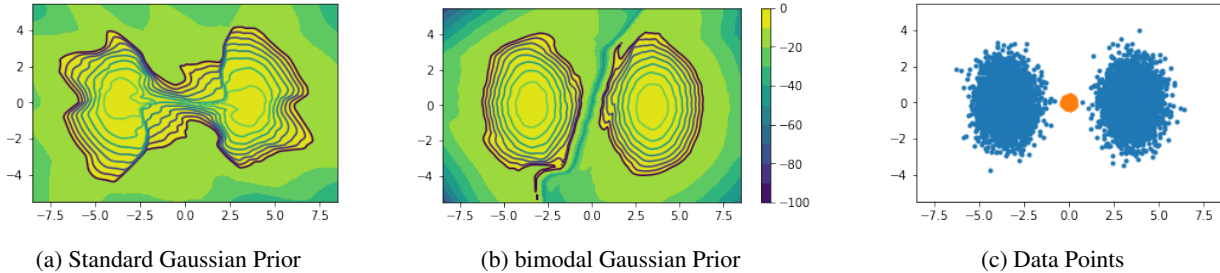


Figure 2: Visualization of the topology mismatch problem on a two-dimensional Gaussian mixture data. (a, b) Contours of the log-likelihoods assigned by flow-based generative models using a standard Gaussian prior and a bimodal Gaussian mixture prior. The 10 contour lines in the images range from -10 to -1. The model with a standard Gaussian prior assigns high likelihoods outside the high probability areas of the true distribution. (c) Training data (blue) and out-of-distribution inputs (orange) used in this experiment.

tion. Figure 1 visualizes the intuition of the mappings from a bimodal data distribution to two different types of prior distributions under our assumptions. If the bimodal data distribution is mapped to a unimodal prior distribution, we cannot eliminate the possibility of the model mapping out-of-distribution inputs to the typical set or high likelihood areas of the prior distribution. We will refer to this issue as the topology mismatch problem. This simple analysis explains the out-of-distribution phenomenon and the results of prior work [24], implying that out-of-distribution inputs can even reside in the typical set. By contrast, if a prior distribution is topologically consistent with the data distribution, there exists a mapping that decreases the possibility of the out-of-distribution phenomenon. Note that we cannot say that the modification in a prior distribution can single-handedly solve the problem as the probability density of latent variables on a prior distribution is not the only factor influencing the likelihood of deep generative models such as VAEs and Glow. In addition, it has been reported that deep generative models trained on similar images can generate dissimilar images [27], and thus our analysis on topology mismatch cannot explain this result. However, we later experimentally show that the choice of the prior distribution nonetheless has a significant influence on the likelihoods assigned to out-of-distribution inputs (Section 5).

To justify our analysis, we conduct experiments on some simple artificial data sets. Figure 2 shows the likelihoods assigned by flow-based deep generative models trained on points sampled from a bimodal Gaussian mixture distribution. We use a simple model architecture with four affine coupling layers and reverse the features after each layer. We compare a unimodal Gaussian prior and a bimodal Gaussian mixture prior. Figure 2 shows that the contours of the log-likelihood assigned by the model using a standard Gaussian prior distribution have high likelihood areas outside the region data points reside. Because the prior distribution is mapped to a distribution with a different topol-

ogy, the mapped distribution will inevitably have undesirable high likelihood areas. By contrast, the contours of the model using a Gaussian mixture prior successfully separates the two modes, and do not have high likelihood areas in out-of-distribution areas. To show that a model with a standard Gaussian prior can assign high likelihood to out-of-distribution inputs even in the low-dimensional case, we compare the likelihoods assigned to out-of-distribution inputs that are points sampled from a Gaussian distribution with mean zero and variance 0.01. As shown in Figure 2c, the out-of-distribution inputs have minimal overlap with the in-distribution data. However, the mean of the log-likelihoods assigned by the model using a standard Gaussian prior to in-distribution inputs is -3.25 , which is similar to the log-likelihood assigned to out-of-distribution inputs (-4.87). By contrast, the mean of log-likelihood assigned to out-of-distribution inputs by the model using a multimodal prior is much lower (-40.11). As the dimensionality of the data increases, this phenomenon becomes more pronounced; however, using a multimodal distribution as a prior can significantly alleviated this problem. Further details are presented in Appendix C.

3.2. Second Order Analysis

Nalisnick *et al.* [23] provided a second order analysis with implications consistent with their experimental observations, while they put some strong assumptions. One implication of their analysis is that deep generative models with unimodal prior distributions assign higher likelihood if out-of-distribution images have lower variance over image pixels. However, since they use a unimodal prior distribution, their analysis do not apply here. To explain why our proposition may help, we perform a similar analysis on assumptions corresponding to our models. Although we still adopt some strong assumptions and apply coarse approximations in a similar manner as the original analysis, our analysis provides an intuitive explanation for our experi-

mental results. The value we are interested in evaluating is

$$\mathbb{E}_q[\log p(\mathbf{x}; \theta)] - \mathbb{E}_{p^*}[\log p(\mathbf{x}; \theta)] \quad (1)$$

where p is a given generative model, q is the adversarial distribution (out-of-distribution), and p^* is the training distribution. If the value of is positive, the adversarial distribution is assigned a higher likelihood by the generative model. In the following analysis, we assume that p reasonably approximates p^* . Note that the analysis for unimodal prior models suggests that q can be assigned higher likelihood even if p perfectly approximates p^* .

Nalisnick *et al.* [23] approximate the probability distribution function of the given generative model p as $\log p(\mathbf{x}; \theta) \simeq \log p(\mathbf{x}_0; \theta) + \nabla_{\mathbf{x}_0} \log p(\mathbf{x}_0; \theta)^T (\mathbf{x} - \mathbf{x}_0) + \frac{1}{2} \text{Tr}\{\nabla_{\mathbf{x}_0}^2 \log p(\mathbf{x}_0; \theta) (\mathbf{x} - \mathbf{x}_0) (\mathbf{x} - \mathbf{x}_0)^T\}$, which is equivalent to assuming that the generative model can be approximated with a Gaussian distribution. In this work, however, we focus on data sets with an underlying distribution which can be approximated by a mixture distribution. Therefore, we assume that p can be approximated as $\log p(\mathbf{x}; \theta) \simeq \log \frac{1}{K} \sum_K p_i(\mathbf{x}; \theta)$, where p_i corresponds to each component approximated by a Gaussian distribution. We assume that each component of the generative model $p_i(\mathbf{x}; \theta)$ corresponds to a component of the prior distribution $p_i(\mathbf{z}; \psi)$.

Here, we adopt the assumption that the generative model is constant-volume Glow (CV-Glow) as is done in [23]. The derivation and detailed assumptions are given in Appendix A. Finally, we derive the following formula:

$$\begin{aligned} & \mathbb{E}_q[\log p(\mathbf{x}; \theta)] - \mathbb{E}_{p^*}[\log p(\mathbf{x}; \theta)] \\ & \simeq -\frac{1}{2\sigma_\psi^2} \sum_{c=1}^C \left(\prod_{l=1}^L \sum_{j=1}^{C_l} u_{l,c,j} \right)^2 \\ & \quad \sum_{h,w} \sum_{i=1}^K (w_i \sigma_{\mathcal{D}_i, h, w, c}^2 - w_i^* \sigma_{\mathcal{D}_i^*, h, w, c}^2) \\ & \leq -\frac{1}{2\sigma_\psi^2} \sum_{c=1}^C \left(\prod_{l=1}^L \sum_{j=1}^{C_l} u_{l,c,j} \right)^2 \\ & \quad \sum_{h,w} (\sigma_{\mathcal{D}_{min}, h, w, c}^2 - \sigma_{\mathcal{D}_{max}^*, h, w, c}^2), \quad (2) \end{aligned}$$

where σ_ψ^2 is the variance of the prior distribution (we assume that all the components have identical variance), \mathcal{D}_i^* and \mathcal{D}_i correspond to the in-distribution and out-of-distribution data allocated to the i -th component and w_i^* , w_i are the ratio of data allocated to the i -th component satisfying $\sum_K w_i^* = 1$, $\sum_K w_i = 1$. $u_{l,c,j}$ is the weight of the l -th 1x1 convolution, which is fixed for any inputs. Further, h and w index the input spatial dimensions, c indexes the input channel dimensions, l indexes the series of flows,

and j indexes the column dimensions of the $C_l \times C_l$ kernel. $\sigma_{\mathcal{D}_i, h, w, c}^2$, $\sigma_{\mathcal{D}_i^*, h, w, c}^2$ are diagonal elements of $\Sigma_{\mathcal{D}_i} = \mathbb{E}[(\mathbf{x} - \bar{\mathbf{x}}_i)(\mathbf{x} - \bar{\mathbf{x}}_i)^T | \mathcal{D}_i]$, $\Sigma_{\mathcal{D}_i^*} = \mathbb{E}[(\mathbf{x} - \bar{\mathbf{x}}_i)(\mathbf{x} - \bar{\mathbf{x}}_i)^T | \mathcal{D}_i^*]$, where $\bar{\mathbf{x}}_i$ is the elementwise mean of the images generated from the i -th component, and the two matrices are assumed to be diagonal. \mathcal{D}_{min} and \mathcal{D}_{max}^* are chosen so the final expression is maximized. Expanding the formula by using CV-Glow does not seem to be a reasonable, as we do not use it in our experiments. However, Nalisnick *et al.* [23] reported that the out-of-distribution phenomenon occurs even on CV-Glow, one of the simplest deep generative models, as with many other more complex deep generative models such as general Glow and VAEs. Therefore, it is worth considering CV-Glow to analyze the problem of general deep generative models.

Roughly speaking, we can say that if $\sigma_{\mathcal{D}_{min}}$ takes smaller values than $\sigma_{\mathcal{D}_{max}^*}$, the likelihood assigned to out-of-distribution data can be larger than that assigned to in-distribution data. However, if this is the case, this indicates that one of the out-of-distribution modes has a mean that is close to the mean of one of the modes of the generative model with small variance. If out-of-distribution data satisfies this condition, such a mode can no longer be considered out-of-distribution, as inputs corresponding to it must be similar to the images corresponding to the mode of the generative model. Note that a mode of the generative model has a small variance and contains similar images under our assumptions. By contrast, the analysis by Nalisnick *et al.* [23] assumed that the data distribution can be approximated by a unimodal Gaussian distribution with possibly large variance. Therefore, low-variance out-of-distribution data with mean identical to in-distribution data can contain completely different images.

Our analysis indicates that the squared distance from the mean of each mode is an important factor of likelihood assignment. We later show that our experimental results are consistent with this analysis. Note that this analysis does not provide an exhaustive explanation for our results, as our experiments show that the squared distance is not the only important factor underlying the likelihood assigned to out-of-distribution inputs (Section 5.3). However, our simple analysis provides an intuitive interpretation of our experimental results similar to the suggestion from the analysis by Nalisnick *et al.* [23].

4. Proposed Model

We replace the prior distributions of deep generative models with mixture distributions $\sum_{i=1}^K p_i/K$ that are not trainable, and we assume that all components are uniformly weighted. Although some previous studies have performed clustering using VAEs with a trainable multimodal prior distribution [7, 33], we manually assign each input to a

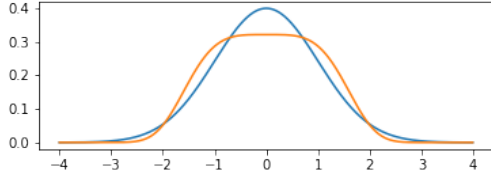


Figure 3: Probability density functions of a standard Gaussian distribution (blue) and a generalized Gaussian distribution with parameters $\alpha = \sqrt{\Gamma(1/\beta)/\Gamma(3/\beta)}$, $\beta = 4$ (orange).

component of the prior distribution before training. We simply use the labels of the data sets or apply k-means clustering on the training data to decide on which components to assign to. During training, the likelihood for each input is evaluated using a different unimodal prior distribution p_i (using a different index i for each input), which is the component of the multimodal prior distribution assigned to each input. The test likelihood is evaluated on a mixture prior distribution $\sum_{i=1}^K p_i/K$ without the component assignment used during training.

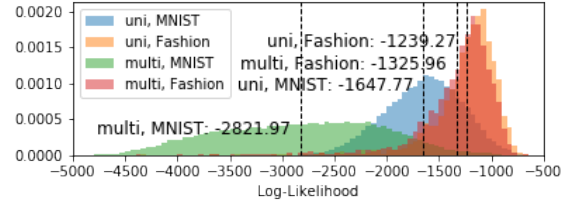
We use Gaussian distributions and generalized Gaussian distributions for the components of the mixture distributions. The probability density function of a univariate generalized Gaussian distribution is

$$p(x; \alpha, \beta) = \frac{\beta}{2\alpha\Gamma(1/\beta)} \exp\left(-\left(\frac{|x - \mu|}{\alpha}\right)^\beta\right) \quad (3)$$

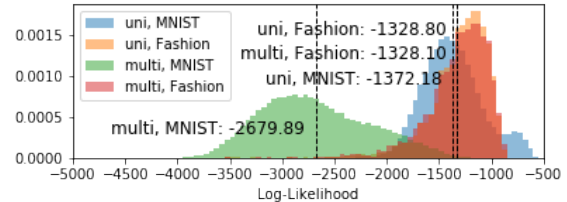
where Γ is the Gamma function and $\alpha, \beta \in (0, +\infty)$ are parameters. The assumption made in our analysis in Section 3.2 suggests that the components of prior distributions should be far from each other and have a small overlap. We observe that Gaussian distributions are too heavy-tailed and components must be placed far away from each other in order to lower the out-of-distribution likelihood. To deal with this problem, we propose the use of a generalized Gaussian distribution. A generalized Gaussian distribution with parameters $\beta = 2$ and $\alpha = \sqrt{2}$ is equal to a standard Gaussian distribution. A generalized Gaussian distribution with large β is light-tailed, so we use a generalized Gaussian distribution with parameters $\alpha = \sqrt{\Gamma(1/\beta)/\Gamma(3/\beta)}$, $\beta = 4$ (Section 5.3). Note that the variance of a generalized Gaussian distribution using $\alpha = \sqrt{\Gamma(1/\beta)/\Gamma(3/\beta)}$ is one.

5. Experiments

We evaluate the effect of a multimodal prior distribution on the likelihoods assigned to out-of-distribution inputs on two pairs of real image data sets: Fashion-MNIST vs. MNIST, and CIFAR-10 vs. SVHN.



(a) VAE



(b) Glow

Figure 4: Histograms of the log-likelihoods assigned by VAEs and Glow trained on Fashion-MNIST (label 1 and 7). “uni” denotes a standard Gaussian prior and “multi” denotes a bimodal Gaussian mixture prior. For Fashion-MNIST, we report likelihoods evaluated on test data. Bimodal priors mitigate the out-of-distribution problem.

5.1. Data Sets

We use two pairs of image data sets. The first pair is Fashion-MNIST [36] (training data) and MNIST [20] (out-of-distribution inputs). The second pair is CIFAR-10 [19] (training data) and SVHN [26] (out-of-distribution inputs). For training, we use a small subset of the data sets, as using all images requires a large number of clusters to lower the out-of-distribution likelihood. For CIFAR-10, 10% random width and height shifting is applied during training as data augmentation.

5.2. Model Architecture and Training Details

Our implementation of VAE is based on the architecture described in [30, 23]. Both the encoder and the decoder are convolutional neural networks. Our implementation of Glow is based on the authors’ code hosted at OpenAI’s open source repository¹. To remove spatial dependencies on the latent variables, we do not use the multi-scale architecture, and apply 1×1 convolution over three dimensions (width, height, channel) after the decoder. Further details are discussed in Appendix B.

5.3. Two Labels and Two Modes

We first analyze our model on simple data sets of images. Here, models are trained on images in label 1

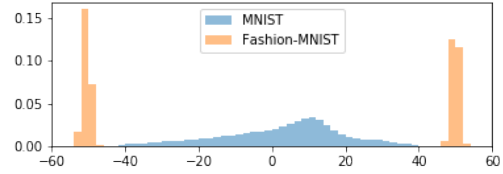
¹<https://github.com/openai/glow>

Model	Prior	Training Data	NLL
VAE	uni	Fashion-MNIST (1, 7)	1647.76
VAE	uni	Fashion-MNIST (1)	1976.73
VAE	uni	Fashion-MNIST (7)	1578.43
VAE	multi	Fashion-MNIST (1, 7)	2821.97
Glow	uni	Fashion-MNIST (1, 7)	1372.18
Glow	uni	Fashion-MNIST (1)	1791.96
Glow	uni	Fashion-MNIST (7)	1595.10
Glow	multi	Fashion-MNIST (1, 7)	2679.89

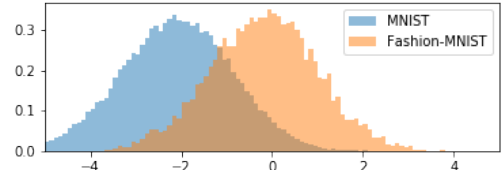
Table 1: Negative log-likelihoods assigned to MNIST by the models trained on Fashion-MNIST. Fashion-MNIST (i) indicates that the model is trained on the images in the i -th label. “uni” denotes a standard Gaussian prior and “multi” denotes a bimodal Gaussian mixture prior. The unimodal prior models trained only on images for one label of Fashion-MNIST still exhibit the out-of-distribution phenomenon for MNIST when compared to multimodal prior models.

(Trouser) and 7 (Sneaker) in Fashion-MNIST. We compare two types of prior distributions: a standard Gaussian distribution and a bimodal Gaussian mixture distribution. The means of the bimodal priors are $[\pm 75, 0, \dots, 0]$ for VAE and $[\pm 50, 0, \dots, 0]$ for Glow. The variances are $\text{diag}([1, \dots, 1])$ on all the components. Figure 4 shows that the models using multimodal prior distributions correctly assign low likelihood to MNIST, the out-of-distribution data, while the models using unimodal prior distributions assign high likelihood to MNIST.

Multi-Modal Priors Force Out Out-of-Distribution Points Our analysis in Section 3.2 suggests that multimodal prior models mitigate the out-of-distribution problem because each component is trained on simpler data. However, although the complexity of data allocated to each component is important, unimodal prior models trained on data allocated to a single component still assign high likelihoods to out-of-distribution inputs when compared to multimodal prior models (Table 1). Figure 5 shows that the model with the multimodal prior correctly places MNIST in an out-of-distribution area within the latent variable space. In contrast, MNIST and Fashion-MNIST (label 7) have large overlap within the latent variable space of the model with a unimodal prior trained only on label 7 of Fashion-MNIST. These results imply that separating in-distribution data in the latent variable space by using a multimodal prior distribution has a strong effect of forcing out-of-distribution points out of high-likelihood areas. This observation suggests a new approach for mitigating the out-of-distribution phenomenon; improving latent variable design.



(a) bimodal, label 1 and 7



(b) Unimodal, label 7

Figure 5: Histograms of the first-idx of the latent variables on Glow trained on label 1 and 7 and the 613rd-idx trained only on label 7 of Fashion-MNIST. For the unimodal prior model, we select the dimension of the latent variable with the largest absolute mean for MNIST. Further results are reported in Appendix F.3.

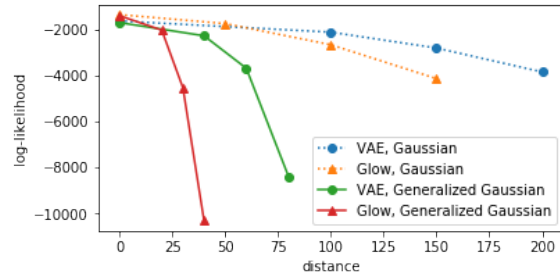
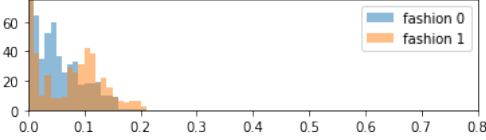
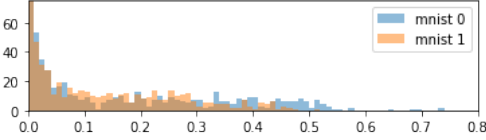


Figure 6: Relationships of the distance between two components and the mean log-likelihoods assigned to MNIST by models trained on Fashion-MNIST (label 1 and 7). While likelihoods assigned to out-of-distribution inputs are sensitive to the distance between components regardless of component choice, the Gaussian mixture priors require much larger distances to lower the likelihood assigned to out-of-distribution inputs. The histograms and the mean values of the log-likelihoods are reported in Appendix F.1

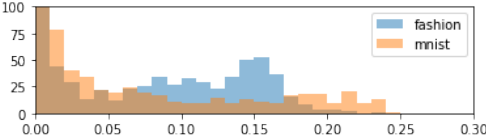
Distance between Two Components We analyze the relationship of the likelihoods assigned to out-of-distribution inputs and the distance between two components using two types of distributions: Gaussian and generalized Gaussian mixture distributions. Figure 6 shows the mean log-likelihoods assigned to MNIST by the models trained on Fashion-MNIST (label 1 and 7) with different types and component distances of prior distributions. Likelihoods assigned to out-of-distribution inputs are sensitive to the



(a) Per-dimensional empirical mean of the squared distance between the mean image of each component of the VAE trained on Fashion-MNIST (label 1 and 7) and images in Fashion-MNIST (label 1 and 7).



(b) Per-dimensional empirical mean of the squared distance between the mean image of each component of the VAE trained on Fashion-MNIST (label 1 and 7) and images in MNIST.



(c) Per-dimensional variance of images in Fashion-MNIST (label 1 and 7) and MNIST

Figure 7: Comparison of the experimental results with the suggestion based on the analysis in Section 3.2. (a), (b) The per-dimensional empirical mean of the squared distance from the mean image of each component of the VAE with a bimodal prior distribution. The model is trained on Fashion-MNIST (label 1 and 7) and test images in Fashion-MNIST (label 1 and 7) and MNIST are assumed to be allocated to the nearest component in the latent variable space. “fashion i ” and “mnist i ” denote the data allocated to the i -th component. (c) The per-dimensional variances over pixels of images in MNIST and Fashion-MNIST. The y-axis is clipped for visualization.

distance between components regardless of the component choice. However, models using Gaussian mixture priors require larger distances to lower the out-of-distribution likelihoods. A generalized Gaussian prior ($\beta = 4$) is particularly effective at assigning low likelihoods to out-of-distribution inputs even with much smaller distances between components. The means of the bimodal distributions are $[\pm d/2, 0, \dots, 0]$, and the variance is $\text{diag}([1, \dots, 1])$ for all the components. Note that the likelihoods assigned to the test data of Fashion-MNIST (label 1 and 7) are relatively unaffected by the distance between two components (Appendix F.1).

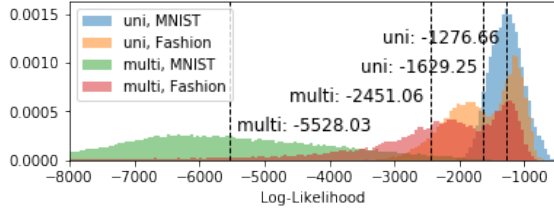
Second Order Analysis Our analysis in Section 3.2 suggests that the conditional expectation of the squared distances from the mean of the images generated from the modes, *i.e.* $\sigma_{\mathcal{D}_i^*, h, w, c}^2, \sigma_{\mathcal{D}_i, h, w, c}^2$, influence the assigned likelihoods. We show that our experimental results are consistent with the analysis. Note that this is not the only influencing factor that lowers the out-of-distribution likelihood as mentioned above. Figure 7a, b show histograms of the per-dimensional empirical mean of the squared distance from the mean of the images generated from each component of the VAE with a bimodal prior distribution, which are the empirical values of $\sigma_{\mathcal{D}_i^*, h, w, c}^2$ and $\sigma_{\mathcal{D}_i, h, w, c}^2$, respectively. The pixel values are scaled to $[0, 1]$. As explained in Section 3.2, we consider each image as allocated to the closest component in the latent variable space, and the squared distance from the mean is calculated over the pixel space. These results are evaluated on the VAE using a bimodal Gaussian mixture prior with means $[\pm 75, 0, \dots, 0]$ trained on Fashion-MNIST (label 1 and 7). Figure 7a, b show that Fashion-MNIST has lower empirical values of $\sigma_{\mathcal{D}_i^*, h, w, c}^2$ compared to those of MNIST $\sigma_{\mathcal{D}_i, h, w, c}^2$. The results are consistent with the implication of our analysis that higher likelihood is assigned if the values are small.

Figure 7c shows the per-dimensional variance of images in Fashion-MNIST (label 1 and 7) and MNIST. In contrast to our analysis, the analysis by Nalisnick *et al.* [23] for unimodal prior models suggests that the models assign higher likelihood to an adversarial distribution if the per-dimensional variance is small. As has been reported in [23], most pixels of images found in MNIST have low variance, and this is consistent with the result that MNIST is assigned higher likelihood when a standard Gaussian prior is used. The differences between these two types of histograms provide an intuitive explanation for the difference between likelihoods assigned to out-of-distribution inputs by models using unimodal and multimodal prior distributions.

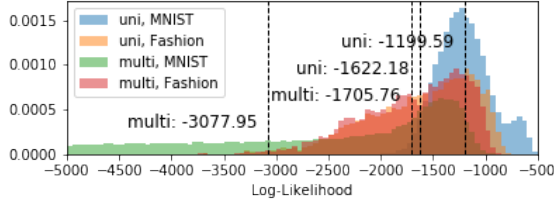
5.4. Results on Complex Data Sets

We evaluate our proposition on more complex data sets. While multimodal priors assign lower likelihoods, the effect is especially limited on Glow. The results on Glow may be affected by the spatial dependencies on the latent variables, and our efforts to remove the dependencies may not be sufficient. Our observations suggest that Glow requires further modifications to solve this problem, so we leave this problem for future work. More investigation into latent variable space as well as separation of data sets is required for further performance. Alternatively, our method can be used in tandem with other techniques such as [12, 24].

Fashion-MNIST (label 0, 1, 7, 8) vs MNIST We evaluate our method on a VAE trained on label 0, 1, 7, and 8. (T-shirt, Trouser, Sneaker, and Bag). We



(a) VAE

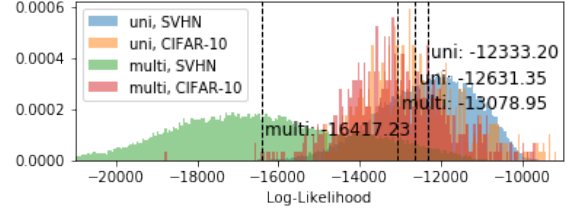


(b) Glow

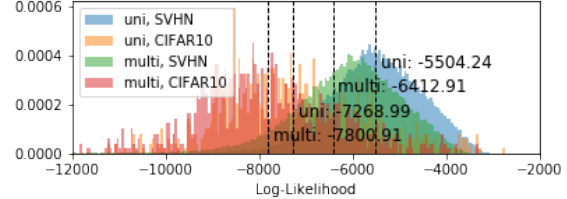
Figure 8: Likelihoods assigned by the models trained on Fashion-MNIST (label 0, 1, 7, 8). The models with uni-modal priors assign higher likelihood to MNIST, whereas those using multimodal priors mitigate this problem.

compare a standard Gaussian prior and a quad-modal Gaussian mixture prior. For the VAE, the means are $[150, 0, \dots, 0]$, $[0, 150, 0, \dots, 0]$, $[0, 0, 150, 0, \dots, 0]$, and $[0, 0, 0, 150, 0, \dots, 0]$. However, we observe that this scheme of placing modes on differing dimensions does not work on Glow. Hence, we use $[200 \times i, 0, \dots, 0]$ ($i = 0, 1, 2, 3$) for Glow. The variances are $\text{diag}([1, \dots, 1])$ for all components. Figure 8 shows that the models using standard Gaussian priors produce the out-of-distribution phenomenon on MNIST, while the models using Gaussian mixture priors do to a lesser degree.

CIFAR-10 (label 0 and 4) vs SVHN We find that images for one label in CIFAR-10 are still too diverse for our method. Therefore, we apply k-means and separate the images in label 0 and 4 of CIFAR-10 into four respective clusters, and we use images in one cluster of each label. We compare the models using a standard Gaussian prior and a bimodal Gaussian mixture prior with means $[\pm 100, 0, \dots, 0]$ for VAE, and $[\pm 200, 0, \dots, 0]$ for Glow. Figure 9 shows that the models with multimodal priors assign lower likelihoods to SVHN compared to the models using unimodal prior distributions. However, this effect is limited on Glow. We hypothesize that images in each cluster are still too diverse for Glow with our settings. These results imply that it is difficult to adopt our method if a data set does not consist of low-variance and distant clusters, and further study is required particularly for Glow.



(a) VAE



(b) Glow

Figure 9: Likelihood assigned by models trained on CIFAR-10 (label 0 and 7). The models using standard Gaussian priors assign higher likelihood to SVHN. The models using multimodal priors mitigate this problem while the effect is limited on Glow.

6. Conclusion and Discussion

We analyzed the influence of prior distribution choice of deep generative models on the likelihoods assigned to out-of-distribution inputs. Recent work [23, 5] on deep generative models with unimodal prior distributions has shown that these models can assign higher likelihoods to out-of-distribution inputs than to training data. In this paper, we showed that models using multi-modal prior distributions lower the likelihoods assigned to out-of-distribution inputs for Fashion-MNIST vs. MNIST and CIFAR10 vs. SVHN. We also provided theoretical explanations for the advantages of the use of multi-modal prior distributions.

Unfortunately, our experimental results suggested that it is difficult to apply our method to complex data sets even when we use prior knowledge. Thus, our work demonstrates the limitation of the high-dimensional likelihoods yet again, and encourages future work on alternative metrics such as [5, 24]. Nevertheless, our work is the first to show that likelihoods assigned to out-of-distribution inputs are affected by the choice of the prior distribution, which has been mainly studied as a way to improve the representative ability of deep generative models for in-distribution data. Our observations motivate further study on the prior distributions of deep generative models, as well as on methods to control the structure of the latent variables to make the model likelihood sensitive to out-of-distribution inputs.

Acknowledgements

This paper has benefited from advice and English language editing from Masayuki Takeda. This work was supported by JSPS KAKENHI (JP19K03642, JP19K00912) and RIKEN AIP Japan.

References

- [1] David Arthur and Sergei Vassilvitskii. k-means++: The Advantages of Careful Seeding. In *ACM-SIAM symposium on Discrete algorithms*, 2007.
- [2] Judith Bütetage, Petra Pokulukar, and Danica Kragic. Modeling assumptions and evaluation schemes: On the assessment of deep latent variable models. In *The IEEE Conference on Computer Vision and Pattern Recognition (CVPR) Workshops*, 2019.
- [3] Francesco Paolo Casale, Adrian V. Dalca, Luca Saglietti, Jennifer Listgarten, and Nicolo Fusi. Gaussian process prior variational autoencoders. In *Conference on Neural Information Processing System (NeurIPS)*, 2018.
- [4] Xi Chen, Diederik P Kingma, Tim Salimans, Yan Duan, Prafulla Dhariwal, John Schulman, Ilya Sutskever, and Pieter Abbeel. Variational Lossy Autoencoder. In *International Conference on Learning and Representation (ICLR)*, 2017.
- [5] Hyunsun Choi, Eric Jang, and Alexander A Alemi. WAIC, but Why? Generative Ensembles for Robust Anomaly Detection. *arXiv preprint arXiv:1810.01392*, 2019.
- [6] Thomas M. Cover and Joy A. Thomas. *Elements of Information Theory*. Wiley-Interscience, 2nd edition, 2006.
- [7] Nat Dilokthanakul, Pedro A M Mediano, Marta Garnelo, Matthew C. H. Lee, Hugh Salimbeni, Kai Arulkumaran, and Murray Shanahan. Deep Unsupervised Clustering with Gaussian Mixture Variational Autoencoders. *arXiv preprint arXiv:1611.02648*, 2016.
- [8] Laurent Dinh, David Krueger, and Yoshua Bengio. NICE: Non-linear Independent Components Estimation. *arXiv preprint arXiv:1410.8516*, 2015.
- [9] Laurent Dinh, Jascha Sohl-Dickstein, and Samy Bengio. Density estimation using Real NVP. In *International Conference on Learning and Representation (ICLR)*, 2017.
- [10] Prasoon Goyal, Zhiting Hu, Xiaodan Liang, Chenyu Wang, and Eric P Xing. Nonparametric Variational Auto-encoders for Hierarchical Representation Learning. In *IEEE International Conference on Computer Vision (ICCV)*, 2017.
- [11] Dan Hendrycks and Kevin Gimpel. A Baseline for Detecting Misclassified and Out-of-Distribution Examples in Neural Networks. In *International Conference on Learning and Representation (ICLR)*, 2017.
- [12] Dan Hendrycks, Mantas Mazeika, and Thomas Dietterich. Deep Anomaly Detection with Outlier Exposure. In *International Conference on Learning and Representation (ICLR)*, 2019.
- [13] Sergey Ioffe and Christian Szegedy. Batch Normalization: Accelerating Deep Network Training by Reducing Internal Covariate Shift. In *International Conference on Machine Learning (ICML)*, 2015.
- [14] Pavel Izmailov, Polina Kirichenko, Marc Finzi, and Andrew Gordon Wilson. Semi-Supervised Learning with Normalizing Flows. In *Workshop on Invertible Neural Networks and Normalizing Flows (ICML 2019)*, 2019.
- [15] Matthew J Johnson, David Duvenaud, Alexander B Wiltschko, Sandeep R Datta, and Ryan P Adams. Composing graphical models with neural networks for structured representations and fast inference. In *Conference on Neural Information Processing Systems (NIPS)*, 2016.
- [16] Diederik P Kingma and Prafulla Dhariwal. Glow: Generative Flow with Invertible 1x1 Convolutions. In *Conference on Neural Information Processing System (NeurIPS)*, 2018.
- [17] Diederik P Kingma and Jimmy Lei Ba. Adam: A Method for Stochastic Optimization. In *International Conference on Learning Representations (ICLR)*, 2014.
- [18] Diederik P Kingma and Max Welling. Auto-Encoding Variational Bayes. In *International Conference on Learning Representations (ICLR)*, 2014.
- [19] Alex Krizhevsky. Learning Multiple Layers of Features from Tiny Images. Technical report, University of Toronto, 2009.
- [20] Yann LeCun, Leon Bottou, Yoshua Bengio, and Patrick Haffner. Gradient-Based Learning Applied to Document Recognition. *Proceedings of the IEEE*, 86(11):2278 – 2324, 1998.
- [21] Shiyu Liang, Yixuan Li, and R Srikant. Enhancing The Reliability of Out-of-distribution Image Detection in Neural Networks. In *International Conference on Learning and Representation (ICLR)*, 2018.
- [22] Vinod Nair and Geoffrey E. Hinton. Rectified Linear Units Improve Restricted Boltzmann Machines, 2010.
- [23] Eric Nalisnick, Akihiro Matsukawa, Yee Whye Teh, Dilan Gorur, and Balaji Lakshminarayanan. Do Deep Generative Models Know What They Don’t Know? In *International Conference on Learning and Representation (ICLR)*, 2019.
- [24] Eric Nalisnick, Akihiro Matsukawa, Yee Whye Teh, and Balaji Lakshminarayanan. Detecting Out-of-Distribution Inputs to Deep Generative Models Using a Test for Typicality. *arXiv preprint arXiv:1906.02994*, 2019.
- [25] Eric Nalisnick and Padhraic Smyth. Stick-Breaking Variational Autoencoders. In *International Conference on Learning Representations (ICLR)*, 2017.
- [26] Yuval Netzer, Tao Wang, Adam Coates, Alessandro Bis-sacco, Bo Wu, and Andrew Y. Ng. Reading Digits in Natural Images with Unsupervised Feature Learning. In *NIPS Workshop on Deep Learning and Unsupervised Feature Learning*, 2011.
- [27] Pramuditha Perera, Ramesh Nallapati, and Bing Xiang. OCGAN: One-class Novelty Detection Using GANs with Constrained Latent Representations. In *IEEE Conference on Computer Vision and Pattern Recognition (CVPR)*, 2019.
- [28] Marco A.F. Pimentel, David A. Clifton, Lei Clifton, and Lionel Tarassenko. A review of novelty detection. *Signal Processing*, 99:215–249, 2014.
- [29] Jason Rolfe. Discrete variational autoencoders. In *International Conference on Learning Representations (ICLR)*, 2017.

- [30] Mihaela Rosca, Balaji Lakshminarayanan, and Shakir Mohamed. Distribution Matching in Variational Inference. *arXiv preprint arXiv:1802.06847*, 2018.
- [31] Alireza Shafaei, Mark Schmidt, and James J. Little. A Less Biased Evaluation of Out-of-distribution Sample Detectors. *arXiv preprint arXiv:1802.06847*, 2018.
- [32] Lucas Theis, Aron Van Den Oord, and Matthias Bethge. A Note on the Evaluation of Generative Models. In *International Conference on Learning and Representation (ICLR)*, 2016.
- [33] Jakub M Tomczak and Max Welling. VAE with a Vamp-Prior. In *International Conference on Artificial Intelligence and Statistics (AISTATS)*, 2017.
- [34] Aron van Den Oord, Nal Kalchbrenner, Oriol Vinyals, Lasse Espeholt, Alex Graves, and Koray Kavukcuoglu. Conditional Image Generation with PixelCNN Decoders. In *Conference on Neural Information Processing Systems (NIPS)*, 2016.
- [35] Aaron van den Oord, Oriol Vinyals, and Koray Kavukcuoglu. Neural Discrete Representation Learning. In *Conference on Neural Information Processing Systems (NIPS)*, 2017.
- [36] Han Xiao, Kashif Rasul, and Roland Vollgraf. Fashion-MNIST: a Novel Image Dataset for Benchmarking Machine Learning Algorithms. *arXiv preprint arXiv:1708.07747*, 2017.

Supplementary Material of “Likelihood Assignment for Out-of-Distribution Inputs in Deep Generative Models is Sensitive to Prior Distribution Choice”

A. Second Order Analysis

In this section, we present detailed explanations for the analysis in Section 3.2. We adopt the assumption that the probability distribution function of the given generative model p can be approximated by mixture distribution $\log p(\mathbf{x}; \theta) \simeq \log \frac{1}{K} \sum_{i=1}^K p_i(\mathbf{x}; \theta)$, where p_i corresponds to each component that can be approximated by a Gaussian distribution. For simplicity, we assume that the components are assigned the uniform weights, and have equal variances. In addition, corresponding to the nature of the data sets that we are considering, we assume that components of the distribution are far from each other and have small variances. Under the assumptions, we can approximate the probability distribution for each input by taking the value from the component that yields the maximum value for the data: $\log p(\mathbf{x}; \theta) \simeq \log \frac{1}{K} \sum_{i=1}^K p_i(\mathbf{x}; \theta) \simeq \max_i \log \frac{1}{K} p_i(\mathbf{x}; \theta)$. Thus, we can write the expectation by the training data distribution p^* as

$$\begin{aligned} \mathbb{E}_{p^*} [\log p(\mathbf{x}; \theta)] &= \sum_{i=1}^K w_i^* \mathbb{E}[\log p(\mathbf{x}; \theta) | \mathcal{D}_i^*] \\ &\simeq \sum_{i=1}^K w_i^* \mathbb{E} \left[\log \frac{1}{K} \sum_{j=1}^K p_j(\mathbf{x}; \theta) \middle| \mathcal{D}_i^* \right] \\ &\simeq \sum_{i=1}^K w_i^* \mathbb{E}[\log p_i(\mathbf{x}; \theta) | \mathcal{D}_i^*] - \log K \end{aligned} \quad (4)$$

where \mathcal{D}_i^* represents in-distribution data allocated to the i -th component and w_i^* is the ratio of data allocated to the i -th component satisfying $\sum_{i=1}^K w_i^* = 1$. We can also expand the expectation by the adversarial distribution q as $\mathbb{E}_q[\log p(\mathbf{x}; \theta)] \simeq \sum_{i=1}^K w_i \mathbb{E}[\log p_i(\mathbf{x}; \theta) | \mathcal{D}_i] - \log K$ where \mathcal{D}_i^* represents out-of-distribution data allocated to the i -th component, and w_i is the ratio of data allocated to i -th component satisfying $\sum_{i=1}^K w_i = 1$.

Since we assume that each component can be approximated by a Gaussian distribution, we use second order approximation for each component: $\log p_i(\mathbf{x}; \theta) \simeq \log p_i(\bar{\mathbf{x}}_i; \theta) + \nabla_{\bar{\mathbf{x}}_i} \log p_i(\bar{\mathbf{x}}_i; \theta)^T (\mathbf{x} - \bar{\mathbf{x}}_i) + \frac{1}{2} \text{Tr}\{\nabla_{\bar{\mathbf{x}}_i}^2 \log p_i(\bar{\mathbf{x}}_i; \theta) (\mathbf{x} - \bar{\mathbf{x}}_i)(\mathbf{x} - \bar{\mathbf{x}}_i)^T\}$. Here, $\bar{\mathbf{x}}_i$ is the mean of images generated from each component. Therefore, $\nabla_{\bar{\mathbf{x}}_i} \log p_i(\bar{\mathbf{x}}_i; \theta)^T (\mathbf{x} - \bar{\mathbf{x}}_i) \simeq 0$ since $\text{argmax}_{\mathbf{x}} \log p_i(\mathbf{x}; \theta) \simeq \bar{\mathbf{x}}_i$. Thus we can expand the

conditional expectation as

$$\begin{aligned} &\mathbb{E}[\log p_i(\mathbf{x}; \theta) | \mathcal{D}_i^*] \\ &\simeq \mathbb{E} \left[\log p_i(\bar{\mathbf{x}}_i; \theta) \right. \\ &\quad \left. + \frac{1}{2} \text{Tr}\{\nabla_{\bar{\mathbf{x}}_i}^2 \log p_i(\bar{\mathbf{x}}_i; \theta) (\mathbf{x} - \bar{\mathbf{x}}_i)(\mathbf{x} - \bar{\mathbf{x}}_i)^T\} \middle| \mathcal{D}_i^* \right] \\ &= \log p_i(\bar{\mathbf{x}}_i; \theta) + \frac{1}{2} \text{Tr}\{\nabla_{\bar{\mathbf{x}}_i}^2 \log p_i(\bar{\mathbf{x}}_i; \theta) \Sigma_{\mathcal{D}_i^*}\} \end{aligned} \quad (5)$$

where $\Sigma_{\mathcal{D}_i^*} = \mathbb{E}[(\mathbf{x} - \bar{\mathbf{x}}_i)(\mathbf{x} - \bar{\mathbf{x}}_i)^T | \mathcal{D}_i^*]$, and it is assumed to be diagonal as in [23]. Furthermore, $\mathbb{E}[\log p_i(\mathbf{x}; \theta) | \mathcal{D}_i] = \log p_i(\bar{\mathbf{x}}_i; \theta) + \frac{1}{2} \text{Tr}\{\nabla_{\bar{\mathbf{x}}_i}^2 \log p_i(\bar{\mathbf{x}}_i; \theta) \Sigma_{\mathcal{D}_i}\}$ where $\Sigma_{\mathcal{D}_i} = \mathbb{E}[(\mathbf{x} - \bar{\mathbf{x}}_i)(\mathbf{x} - \bar{\mathbf{x}}_i)^T | \mathcal{D}_i]$. Note that $\Sigma_{\mathcal{D}_i^*}$ and $\Sigma_{\mathcal{D}_i}$ are not the variance matrices as $\bar{\mathbf{x}}_i$ are the mean images of the generative model.

Because we assume that variances of all components are identical, $\log p_i(\bar{\mathbf{x}}_i; \theta)$ can be approximated to be identical for all i . Finally, we can write the difference of the two log-likelihoods (Equation 1) in a relatively simple form in parallel with the first line of Equation 5 in [23]:

$$\begin{aligned} &\mathbb{E}_q[\log p(\mathbf{x}; \theta)] - \mathbb{E}_{p^*}[\log p(\mathbf{x}; \theta)] \\ &\simeq \sum_{i=1}^K w_i \mathbb{E}[\log p_i(\mathbf{x}; \theta) | \mathcal{D}_i] \\ &\quad - \sum_{i=1}^K w_i^* \mathbb{E}[\log p_i(\mathbf{x}; \theta) | \mathcal{D}_i^*] \\ &= \frac{1}{2} \text{Tr} \left\{ \sum_{i=1}^K w_i \nabla_{\bar{\mathbf{x}}_i}^2 \log p_i(\bar{\mathbf{x}}_i; \theta) \Sigma_{\mathcal{D}_i} \right. \\ &\quad \left. - \sum_{i=1}^K w_i^* \nabla_{\bar{\mathbf{x}}_i}^2 \log p_i(\bar{\mathbf{x}}_i; \theta) \Sigma_{\mathcal{D}_i^*} \right\}. \end{aligned} \quad (6)$$

If we assume that each p_i is precisely a Gaussian distribution, we can simply compute the Hessian in Equation 6. However, because this assumption is too strong, Nalisnick *et al.* [23] expanded this formula by adopting the assumption that the generative model is constant-volume Glow (CV-Glow). Although we do not use CV-Glow in our experiments, we apply the expression derived by Nalisnick *et al.* [23]:

$$\begin{aligned} &\text{Tr} \left\{ \nabla_{\bar{\mathbf{x}}_i}^2 \log p_i(\bar{\mathbf{x}}_i; \theta) \Sigma_{\mathcal{D}_i} \right\} \\ &= -\frac{1}{2\sigma_\psi^2} \sum_{c=1}^C \left(\prod_{l=1}^L \sum_{j=1}^{C_l} u_{l,c,j} \right)^2 \sum_{h,w} \sigma_{\mathcal{D}_i, h, w, c}^2 \end{aligned} \quad (7)$$

where σ_ψ^2 is the variance of a component of the prior distribution (we assume all components have identical variance) and $\sigma_{\mathcal{D}_i, h, w, c}^2$ are diagonal elements of $\Sigma_{\mathcal{D}_i}$. $u_{l,c,j}$ is the weight of the l -th 1x1 convolution of Glow, which is fixed

for any inputs. h and w index the input spatial dimensions, c indexes the input channel dimensions, l indexes the series of flows, and j indexes the column dimensions of the $C_l \times C_l$ kernel. We assume that each component of the generative model $p_i(\mathbf{x}; \theta)$ corresponds to a component of prior distribution $p_i(\mathbf{z}; \psi)$. Finally, we arrive Equation 2.

B. Experimental Settings

We present model architectures and training settings of the experiments shown in Section 5.

VAE Our implementation of VAE [18] is based on the architecture described in [30, 23]. Both the encoder and the decoder are convolutional neural networks described in Table 2 and 3. We use batch normalization [13] after every convolutional layer except for the last layer of the encoder and the decoder. All the convolutional layers in the decoder use ReLU [22] as an activation function after batch normalization. After the final layer of the decoder, we apply the softmax function, and assume i.i.d. categorical distributions on pixels as visual distributions.

We perform training for 1,000 epochs using the Adam optimizer [17] ($\beta_1 = 0.5, \beta_2 = 0.9$) with a constant learning rate of $1e-3$. We use 5,000 sample points to approximate test likelihoods.

Operation	Kernel	Strides	Channels	Pad
Convolution	5×5	2	8	1
Convolution	5×5	1	16	1
Convolution	5×5	2	32	1
Convolution	5×5	1	64	1
Convolution	5×5	2	64	1
Fully-Connected	—	—	50×2	—

(a) Encoder. The outputs are means (50) and log variances (50).

Operation	Kernel	Strides	Channels	Pad
Fully-Connected	—	—	3136	—
Reshape	—	—	64	—
Convolution	5×5	2	64	2
Convolution	5×5	2	32	1
Convolution	5×5	1	64	1
Convolution	4×4	1	256	1

(b) Decoder. “Convolution” in the decoder is transposed convolution. The reshape operation reshape the latent variables sized 3, 136 to $7 \times 7 \times 64$.

Table 2: Model architecture of VAE for Fashion-MNIST and MNIST. “Channels” denotes the size of the output channel, and “Pad” denotes paddings.

Glow For our experiments of Glow [16], our implementation is based on the code hosted at OpenAI’s open source repository². For Fashion-MNIST vs. MNIST, we use 1 block of 32 affine coupling layers, squeezing the spatial dimension after the 16-th layer. For CIFAR-10 vs. SVHN, we use 1 block of 24 affine coupling layers, squeezing the spatial dimension after the 8-th and 16-th layer.

To alleviate the spatial dependencies on the latent variables, we do not use the multi-scale architecture, which splits the latent variables after squeezing [9]. In addition, we apply 1×1 convolution over three dimensions (width, height, channel) after the encoder, and apply the inverse operation before the decoder. In the implementation, we add the code in Listing 1 after the encoder, and add the inverse operation before the decoder. Moreover, we add a small positive value (0.1 in our implementation) to the scale of affine coupling layers to stabilize the training as suggested at ³. While Nalisnick *et al.* [23] remove actnorm and apply their original initialization scheme, we use actnorm and apply the original initialization scheme in the OpenAI’s code.

We perform training for 1,000 epochs using the Adam optimizer in accordance with the OpenAI’s code. We use a learning rate of $1e-3$, which is linearly annealed from zero over the first 10 epochs.

Operation	Kernel	Strides	Channels	Pad
Convolution	5×5	2	8	1
Convolution	5×5	1	16	1
Convolution	5×5	2	32	1
Convolution	5×5	1	64	1
Convolution	5×5	2	64	1
Fully-Connected	—	—	100×2	—

(a) Encoder. The outputs are means (50) and log variances (50).

Operation	Kernel	Strides	Channels	Pad
Convolution	4×4	1	64	0
Convolution	4×4	2	32	1
Convolution	4×4	2	32	1
Convolution	4×4	2	256×3	1

(b) Decoder. “Convolution” in the decoder is transposed convolution. The reshape operation reshapes the latent variables sized 3, 136 to $7 \times 7 \times 64$.

Table 3: Model Architecture of VAE for CIFAR-10 and SVHN. “Channels” is the size of output channel, and “Pad” is paddings.

```

1 z = tf.transpose(z, perm=[0, 3, 2, 1])
2 z, logdet = invertible_1x1_conv("invconv1", z,
   logdet)
3 z = tf.transpose(z, perm=[0, 3, 2, 1])
4 z = tf.transpose(z, perm=[0, 1, 3, 2])
5 z, logdet = invertible_1x1_conv("invconv2", z,
   logdet)
6 z = tf.transpose(z, perm=[0, 1, 3, 2])
7 z, logdet = invertible_1x1_conv("invconv3", z,
   logdet)

```

Listing 1: Code added for permutation after the encoder of Glow to remove the spacial dependencies on latent variables. The inverse operation is added before the decoder.

C. Simple Artificial Data

For artificial data used in Section 3.1, we compare the likelihoods assigned to in-distribution and out-of-distribution data to show that a standard Gaussian prior can assign high likelihoods to out-of-distribution inputs. The in-distribution data is generated from a two-dimensional Gaussian mixture distribution whose means are $[\pm 3.5, 0]$ and variance is $\text{diag}([0.5, 1])$, and the out-of-distribution data is sample points from a two-dimensional Gaussian distribution with zero mean and 0.01 variance. Figure 2c shows that out-of-distribution inputs does not have any overlap with in-distribution data. However, Figure 10a shows that the log-likelihoods assigned for in-distribution and out-of-distribution inputs by the model using a standard Gaussian prior are similar. On the contrary, the model using a multimodal prior distribution assigns much lower likelihoods to out-of-distribution inputs.

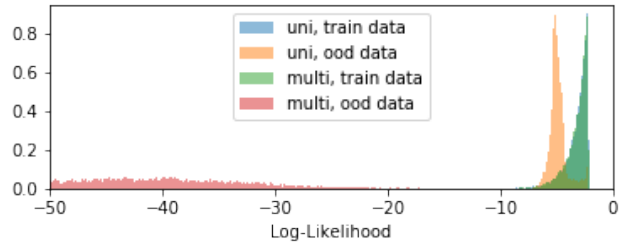
This phenomenon is more serious for high dimensional data. The in-distribution data is generated from a 10 dimensional Gaussian mixture distribution whose means are $[\pm 3.5, 0, \dots, 0]$ and variances are $\text{diag}([0.5, 1, \dots, 1])$ for both components. The out-of-distribution data is generated from a 10 dimensional Gaussian distribution with zero mean and 0.01 variance. Figure 10b, c shows that the log-likelihoods assigned by the model using a standard Gaussian prior assigned to out-of-distribution inputs are much higher than those assigned to in-distribution data, although the model using a multimodal prior assigns much smaller likelihoods to out-of-distribution inputs.

D. Mean Images of Clusters

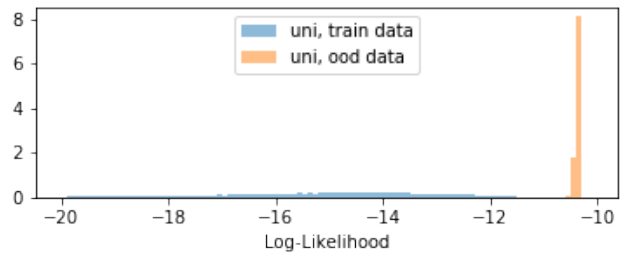
Figure 11 shows the images corresponding to the means of components of the bimodal prior distributions of VAE and Glow trained on label 0 and 7 of Fashion-MNIST. The means are $[\pm 75, 0, \dots, 0]$ on the VAE, and $[\pm 50, 0, \dots, 0]$

²<https://github.com/openai/glow>

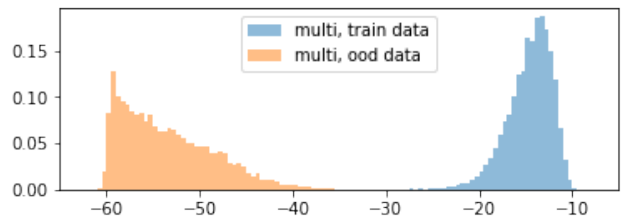
³<https://github.com/openai/glow/issues/40>



(a) 2 dimensional data



(b) 10 dimensional data, Standard Gaussian prior



(c) 10 dimensional data, multimodal prior

Figure 10: (a) Histograms of the log-likelihoods assigned to training and out-of-distribution data by flow-based generative models trained on simple two-dimensional Gaussian mixture data in Section 3.1. “uni” denotes a unimodal prior, and “multi” denotes a multimodal prior. While a model with a unimodal prior assigns relatively high likelihoods to out-of-distribution inputs, a model with a multimodal prior assigns much lower likelihoods to out-of-distribution inputs. (b, c) The histograms of the log-likelihoods assigned by flow-based generative models for 10 dimensional data. The out-of-distribution problem is more serious for high-dimensional data.

on the Glow. Figure 12 shows the images corresponding to the means of the unimodal prior distributions of the VAE and Glow. The mean images of the a bimodal prior VAE are similar to the images in each cluster. However, the mean image of the standard Gaussian prior VAE is different from the training data. For Glow with a standard Gaussian prior, while the mean image is similar with in-distribution data, some images from random sampling of Glow are different from the training data. The results suggests that the models with unimodal prior distribution can assign high likeli-

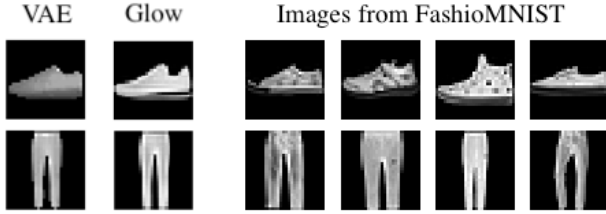


Figure 11: Images corresponding to the means of components of the bimodal prior distributions of VAE and Glow trained on label 0 and 7 of FashionMNIST (left). Images in the data set allocated to each cluster (right).

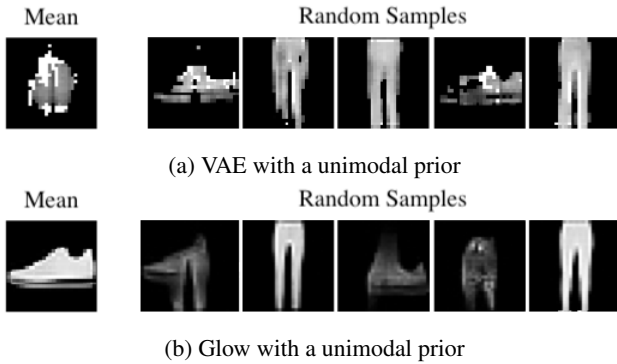
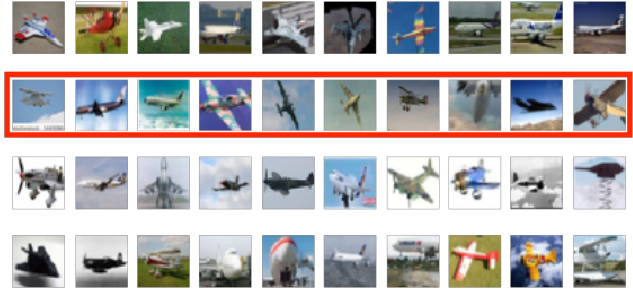


Figure 12: Images corresponding to the means of the unimodal distributions of VAE and Glow trained on label 0 and 7 of Fashion-MNIST (left), and images generated from random sampling (right). The mean image of VAE is dissimilar with training data while image from random sampling are similar with training data. While the mean image of Glow is similar to training data, some images from random sampling of Glow are dissimilar with training data.

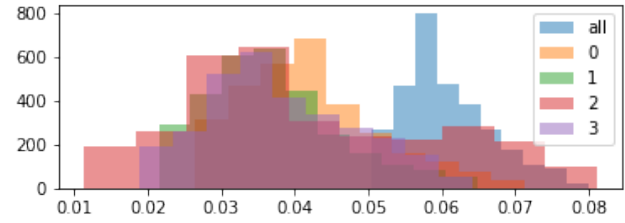
hoods to out-of-distribution inputs because they can contain out-of-distribution inputs in their high likelihood areas or typical sets.

E. K-means Clustering for CIFAR-10

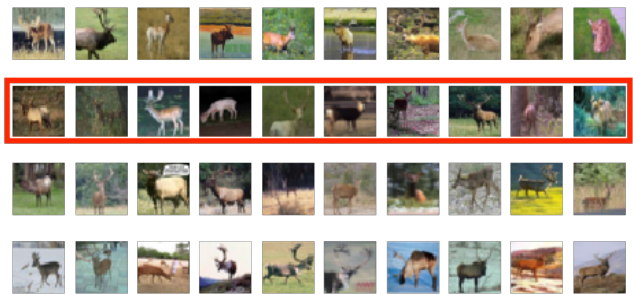
In the experiments reported in Section 5.4, we separate the images in label 0 and 4 of CIFAR-10 by k-means clustering ($k = 4$) initialized by k-means++ [1] respectively. Figure 13 shows sample images from the clusters and the per-dimensional variance of the images in each cluster. The histograms show that k-means clustering successfully decreases the per-dimensional variance. In our experiments, we use images in the cluster corresponding to the second rows.



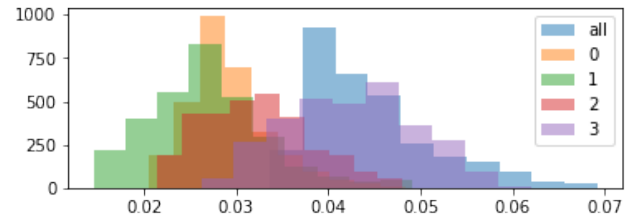
(a) Sample images in four clusters of label 0. Each row corresponds to one cluster. We use the images in the second row.



(b) Per-dimensional variance of images in each cluster of label 0.



(c) Sample images in four clusters of label 4. Each row corresponds to one cluster. We use the images in the second row.



(d) Per-dimensional variance of images in each cluster of label 4.

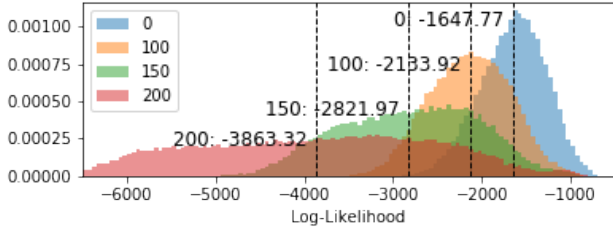
Figure 13: K-means clustering for CIFAR-10 label 0 and 4.

F. Additional Experimental Results

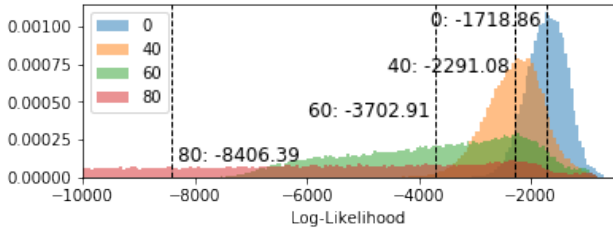
We show additional materials for the results reported in Section 5.

F.1. Distance between Two Components

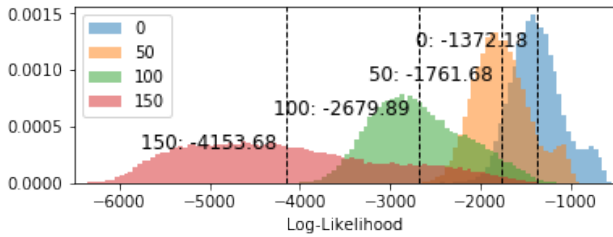
Figure 14, 15 show the histograms of the log-likelihoods assigned to MNIST and the test data of Fashion-MNIST (label 1, 7) by Glow and VAEs trained on Fashion-MNIST



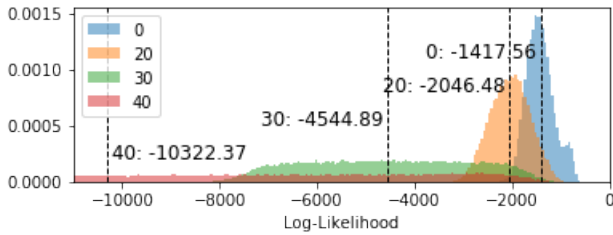
(a) VAE, Gaussian mixture



(b) VAE, Generalized Gaussian mixture



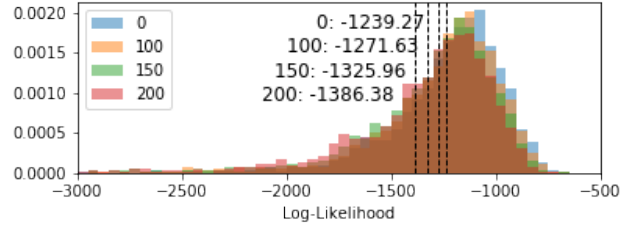
(c) Glow, Gaussian mixture



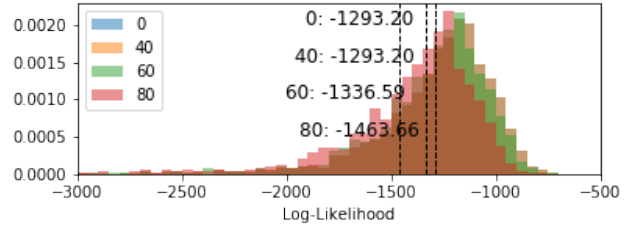
(d) Glow, Generalized Gaussian mixture

Figure 14: Distances between two components and log-likelihoods assigned to MNIST by models trained on Fashion-MNIST (label 1 and 4). The results in these images correspond to those in Figure 6.

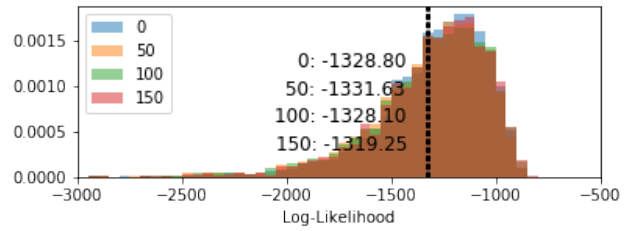
(label 1, 7) using different distances between two components. Figure 14 shows the histograms corresponding to the results reported in Figure 6. The likelihoods assigned to the test data of Fashion-MNIST are not affected by the distances between two components significantly compared to those assigned to MNIST.



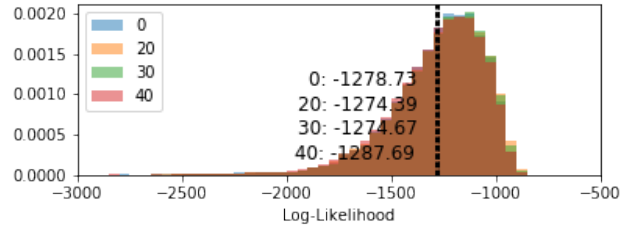
(a) VAE, Gaussian mixture, Fashion-MNIST (1, 7)



(b) VAE, Generalized Gaussian mixture, Fashion-MNIST (1, 7)



(c) Glow, Gaussian mixture, Fashion-MNIST (1, 7)

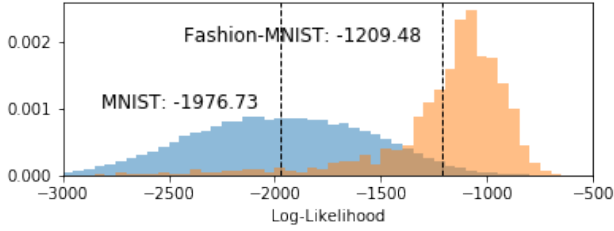


(d) Glow, Generalized Gaussian mixture, Fashion-MNIST (1, 7)

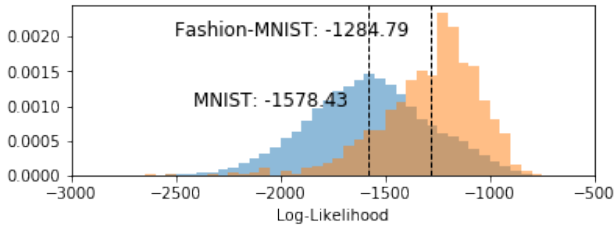
Figure 15: Distances between two components and the log-likelihoods assigned to test data (Fashion-MNIST (1, 7)) by VAEs trained on Fashion-MNIST (1, 7). The likelihoods assigned to the test data are relatively not affected by the distance between two components.

F.2. unimodal Prior Models Trained on Simpler Data

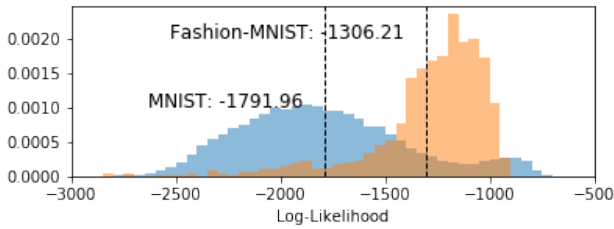
Figure 16 shows the log-likelihoods assigned to MNIST and the test data by models with standard Gaussian priors trained on Fashion-MNIST (label 1 or 7). Although the models assign lower likelihood to MNIST, the effect of alleviating the out-of-distribution behaviour is not significant compared to that of the model using a multimodal prior.



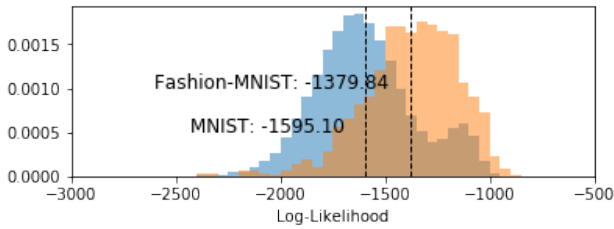
(a) VAE, label 1



(b) VAE, label 7



(c) Glow, label 1

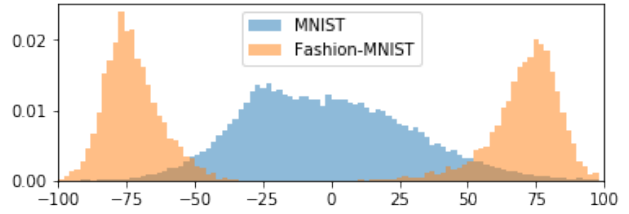


(d) Glow, label 7

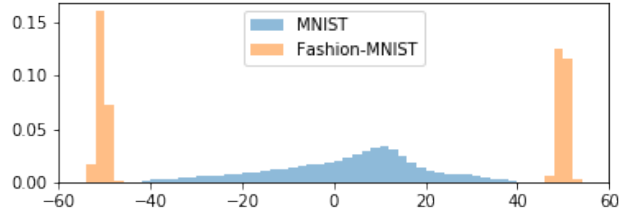
Figure 16: Histograms of the log-likelihoods assigned by models with standard Gaussian priors trained on Fashion-MNIST (label 1 or 7). The results corresponds to those in Table 1. While the models trained on a simpler data set assign lower likelihoods to out-of-distribution inputs, the models using multimodal distributions assign much lower likelihoods.

F.3. Histograms of the Latent Variables

Figure 17 shows the histograms of the latent variables of the models with bimodal prior distributions trained on Fashion-MNIST (label 1, 7). For the results on VAE, we show the histograms of the means of posterior distributions. Figure 19 shows the histograms of the latent variables on the

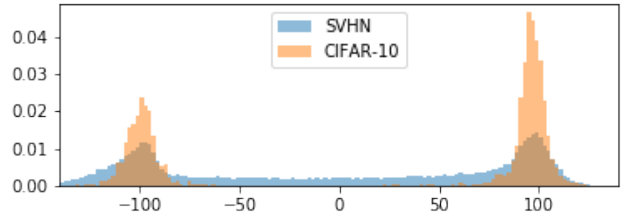


(a) VAE

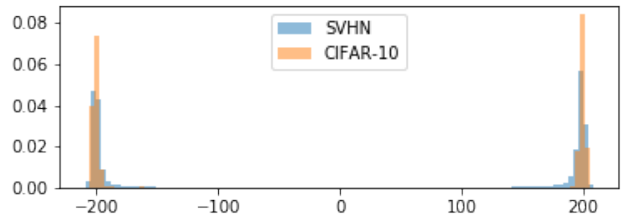


(b) Glow

Figure 17: Latent variables on the models with bimodal Gaussian priors trained on Fashion-MNIST (label 1, 7). The latent variables of MNIST reside in out-of-distribution areas.



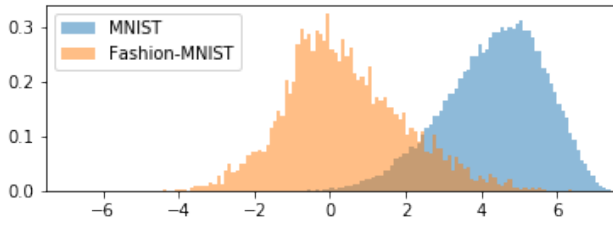
(a) VAE



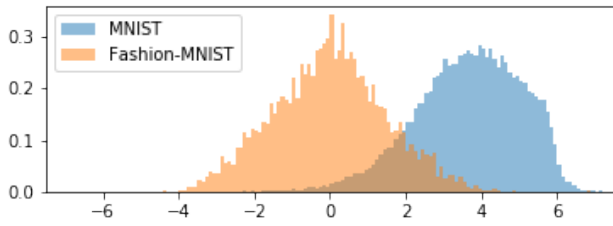
(b) Glow

Figure 18: Latent variables on the models with bimodal Gaussian priors trained on CIFAR-10 (label 0, 4). The latent variables of SVHN reside near in-distribution areas.

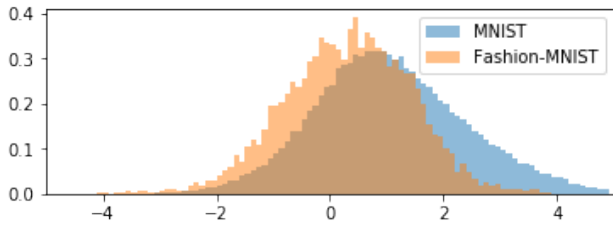
models with standard Gaussian priors trained on Fashion-MNIST (label 1 or 7). In the latent variable spaces of the models with multimodal prior distributions, MNIST resides in out-of-distribution areas and it does not have a large overlap with Fashion-MNIST. By contrast, while we select the



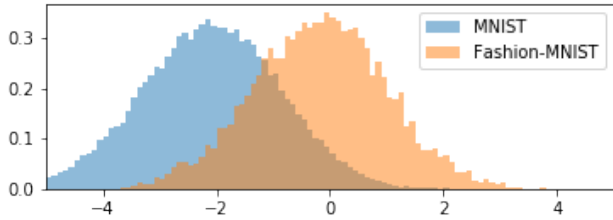
(a) VAE, label 1



(b) VAE, label 7



(c) Glow, label 1



(d) Glow, label 7

Figure 19: Histograms of the latent variables on the models with standard Gaussian prior trained on Fashion-MNIST label 1 or 7. We select the dimension whose mean of the latent variables of MNIST is farthest from zero.

dimension whose mean of the latent variables of MNIST is farthest from zero (the mean of the prior distributions), the latent variables of MNIST have a large overlap with those of Fashion-MNIST on the models with unimodal prior distributions, especially on Glow.

Figure 18 shows the histograms of the latent variables of the models with bimodal prior distributions trained on CIFAR-10 (label 0, 4). In contrast to Fashion-MNIST vs. MNIST, the latent variables of SVHN are located near the in-distribution areas.